Polarization-Insensitive Silicon Nitride Photonic Receiver Based on Thin Waveguides for Optical Interconnects At 1 μm

Citation for the original published paper (version of record):
Caut, A., Karlsson, M. (2024). Polarization-Insensitive Silicon Nitride Photonic Receiver Based on Thin Waveguides for Optical
Interconnects At 1 μm. IEEE Photonics Journal, 16(2): 1-7.
http://dx.doi.org/10.1109/JPHOT.2024.3361802

(article starts on next page)

Polarization-insensitive Silicon Nitride Photonic Receiver based on Thin Waveguides for Optical Interconnects at 1 μm

Alexander Caut and Magnus Karlsson, *Fellow Optica, Fellow IEEE*
Photonics Laboratory, Department of Microtechnology and Nanoscience, Chalmers University of Technology, SE-412 96 Göteborg, Sweden

***Abstract*—This paper demonstrates with simulations two polarization independent wavelength division multiplexing receiver platforms based on thin silicon nitride waveguides for optical interconnects at 1 μm. The chosen waveguide base geometry (width = 900 nm $\times$ height = 160 nm) is a good tradeoff between mode confinement and propagation loss. We first propose a design using a polarization splitter with an 1×4 demultiplexer based on an arrayed waveguide grating (AWG). This receiver has a reduced size and requires only one etching step. We later propose another simplified receiver design using a polarization splitter-rotator with two identical 1×4 demultiplexers based on cascaded Mach-Zehnder interferometers. The rotator is based on a thicker waveguide (width = 500 nm $\times$ height = 400 nm) and is partially etched to rotate the electric field by 90°. Thus, it requires the use of mode size converters at the in/output ports. To keep the fabrication complexity as low as possible for the second design, we limited ourselves to only two etching steps. Therefore, the thickness of the slab of the mode converters and of the rotator is the same as for the main 900 nm (wide) $\times$ 160 nm (thick) waveguide. The simulated extinction ratio of the polarization splitter at 1035 nm is 18 dB and the calculated TM-TE and TE-TM polarization conversion efficiency of the polarization rotator at 1035 nm is 99.9%.**

***Index Terms*—Optical interconnects, Silicon nitride, arrayed waveguide grating, Mach-Zehnder interferometer, coupling loss, polarization dependence, fiber misalignment, manufacturing tolerance.**

I. Introduction

Polarization independence is a crucial factor for the receiver side of an optical interconnect as the polarization of the out-coupled light from a single-mode fiber is unknown and eventually drifts with time. Several ways exist to achieve polarization tolerance and the simplest one consists in designing square waveguides to obtain equal effective indices for the fundamental TE_{00} and TM_{00} modes. However, the use of square single mode waveguides results in a strong interaction of the propagating mode with the sidewalls [1]. As one of the main source of propagating loss in a waveguide is the sidewall roughness, there is a tradeoff between thick polarization insensitive waveguides and thin low loss waveguides [1], [2], [3]. In addition, the use of square waveguide could still result in polarization diversity as fabrication deviations in the core geometry occur [4]. In Ref [1], two single-mode waveguides had been designed: one had a dimension of 800 nm $\times$ 740 nm (width $\times$ height) and another 1500 nm $\times$ 200 nm. The measured propagation loss was 30 dB/m for the quasi-square waveguide and 4.1 dB/m for the thin waveguide. This makes the thin waveguide more attractive for low loss operation. However, in such waveguide design, the guided mode is much less confined and leads to a higher critical bending radius [1], [2], [3]. In addition, thin waveguides are polarization sensitive and require additional components such as polarization splitters and rotators to make the receiver polarization independent [5], [6]. This would increase the size of the whole integrated receiver with respect to one based on square waveguides. Despite this, thin waveguides are of interest as a receiver based on square waveguides would require good tolerance to fabrication defects which could potentially lead to unwanted polarization diversity. In Ref [7], a TE/TM polarization shift of 1.6 nm was observed in the cascaded Mach Zehnder interferometer based on a 600 nm $\times$ 600 nm waveguide for a channel spacing of 20 nm.

In our envisioned receiver platform, the wavelengths are demultiplexed into photodiode arrays, flip-chipped over grating couplers which are more tolerant to misalignment than edge couplers [3]. With the recent development of efficient GaAs VCSEL emitting at 1060 nm [8], [9], [10] and the reduced dispersion and propagation losses in optical fibers at this wavelength [11], the 1 micron band (1015-1055 nm) would allow a reduction of cost and power consumption [3]. This paper further extends the research done in our previous work [3], [12] and focuses on the receiver side, and to the best of our knowledge, investigation of polarization independent receivers at 1 μm is still missing. Silicon nitride (Si_3N_4) is the material of choice as it is transparent from the visible to the mid infrared [13] and presents a good tradeoff between footprint and phase errors compared to other technologies based on silicon and silica due to its moderately low refractive index contrast [14]. In addition, Si_3N_4 is CMOS compatible.

For the demultiplexing device (DEMUX), arrayed waveguide gratings (AWGs) could be considered due to their small footprint [15]. One common approach to make the AWG insensitive to polarization variations is the use of a polarization splitter at the input waveguide of the device [16]. Another innovative possibility is to insert polarization rotators in the arrayed waveguides of the AWG, making the device insensitive to polarization change [17]. In this work, we propose two polarization independent receiver designs based on a thin waveguide. The selected dimension of the waveguide is 900 nm $\times$ 160 nm (width $\times$ height). This geometry was already

selected in our previous work for 1 μm components [3]. Demultiplexers based on AWGs and cascaded Mach-Zehnder interferometers (MZIs) at 1 μm with a channel spacing of 25 nm were demonstrated in Ref [15]. In this work, we envision on the transmitter side VCSELs manufactured in the same array to significantly reduce the footprint and to increase the bandwidth density [12]. However, since the gain bandwidth of the VCSEL is limited [10], the channel spacing has to be reduced. Therefore, an array containing 4 VCSELs emitting at different wavelengths needs to have a channel separation of 8 nm. The wavelengths of the VCSELs are located at 1023, 1031, 1039 and 1047 nm.

The paper is organized as follows: Section II describes a polarization independent receiver design based on a polarization splitter and an arrayed waveguide grating (AWG). Then section III further exploits the polarization splitter by proposing another design based on a polarization splitter-rotator and two identical cascaded MZIs. Finally, Section IV presents discussions followed with conclusions.

II. Receiver based on an AWG with a polarization splitter

This section focuses on TM-TE polarization conversion based on edge coupling between the fiber and the thin waveguide. We explore the polarization splitter, the polarization rotator and the different combinations with a demultiplexer and grating couplers to obtain a polarization independent platform.

Integrated receivers play a key role in data communication and WDM is crucial for high network capacity. WDM photodiodes with high-speed output of 100 Gbit/s have been demonstrated and feature low-loss AWGs based on Silicon technology [18]. In our previous work, we designed and demonstrated SiN integrated devices in the 1 micron band based on a 900 nm x 160 nm (width $\times$ thickness) waveguide [3]. The measured propagation loss was below 0.3 dB/cm [3] and mainly arise from sidewall roughness and fabrication quality. In this work, we chose to conserve the same waveguide dimensions as they present a good tradeoff between propagation loss, mode confinement and reduced footprint. The effective indices for the TE_{00} and TM_{00} modes are respectively 1.567 and 1.491 and the simulated differential group delay with Finite Difference Time Domain (FDTD) was estimated to be 6.5×10^{-4} ps/μm, which corresponds to a delay of 1.3 ps for a 2 mm-long receiver. The buried oxide SiO_2 layer can be thermally deposited on top of a silicon wafer, with a thickness of 3 μm. The 160 nm thick Si_3N_4 can be deposited with a low-pressure chemical vapor deposition (LPCVD) method. The top SiO_2 cladding can be deposited with LPCVD with a thickness of 3 μm.

One common approach is the use of an AWG with two inputs, each corresponding to one specific polarization. As the effective index differs between the fundamental TE and TM modes, they will have a different initial phase at the input of the 1st free propagation region (FPR). Therefore, to compensate this initial difference and to make the AWG polarization independent, the TM input is angularly shifted from the TE input, which will result in a matching between the two spectra. Thus, the AWG requires a polarization splitter prior to the device to separate the TE and TM modes and guide them at their assigned input. The design presented is conventional and directional coupler-based. As the TE_{00} mode is more confined than the TM_{00} mode, it can be guided in curved waveguides with a bending radius below 50 μm with minor losses. The TM_{00} mode however, requires a bending radius above 200 μm to be properly confined. Figure 1a shows the scheme of the receiver based on a polarization splitter and the AWG. The TE and TM input of the AWG are angularly shifted. Since grating couplers are polarization dependent, and that the propagating mode coming from each channel could be either TE or TM polarized, edge couplers are only considered. Figure 1b shows a scheme of the polarization splitter. The TE and TM polarization are guided into the bar and cross output respectively. The device was designed and optimized with FDTD simulations. Figures 1c and d show the electric field profiles of the polarization splitter when the input polarization is TE and TM respectively. Figure 1e presents the transmission of the polarization splitter when the input is a TE_{00} or a TM_{00} mode. The blue and orange continuous curves represent the transmitted power of the TE polarization at the bar and cross output respectively. The blue and orange dashed curves on the other hand represent the transmitted power of the TM polarization at the bar and cross output respectively. The device has a good transmission for both polarizations: -0.1 and -0.3 dB for the TE and TM polarization respectively at 1035 nm.

The extinction ratio (ER) of the device is defined as [19], [20]

$$ER_{Bar} = \log_{10} \frac{TE_{Bar}}{TM_{Bar}} \tag{1}$$

$$ER_{Cross} = \log_{10} \frac{TM_{Cross}}{TE_{Cross}} \tag{2}$$

The ER of the polarization splitter is plotted in Figure 1f. The simulated ER for the bar and cross output is 16 and 18 dB respectively. The crosstalk and wavelength dependence of the device can be reduced by curving the waveguides but at the cost of increasing significantly the device's footprint.

Figure 1g shows the simulated response of the AWG for the TE (continuous curve) and the TM polarization (dashed curve). The simulations were carried out with 2D Beam Propagation Method (2D BPM). The base length difference between the arrayed waveguides is 18.6 μm and the designed free spectral range (FSR) is 32 nm. The separation between the TE and TM input waveguides at the interface of the input free propagation region (FPR) is 2.6 μm. However, the output waveguide spacing is larger on the second FPR and is set at 4.6 μm. The length of both FPRs is 51.4 μm and the separation between them is 800 μm. The AWG has a footprint of 800 μm $\times$ 700 μm excluding the input and output waveguides and the whole receiver an estimated footprint of 1800 μm $\times$ 1300 μm. The device works reasonably well with a slight channel mismatch of around 1 nm which is due to polarization dispersion in the FPRs and in the arrayed waveguides[16]. The method proposed in Ref [16] consists in adapting the width of the arrayed waveguides so that the effective and group index

This article has been accepted for publication in IEEE Photonics Journal. This is the author's version which has not been fully edited and content may change prior to final publication. Citation information: DOI 10.1109/JPHOT.2024.3361802

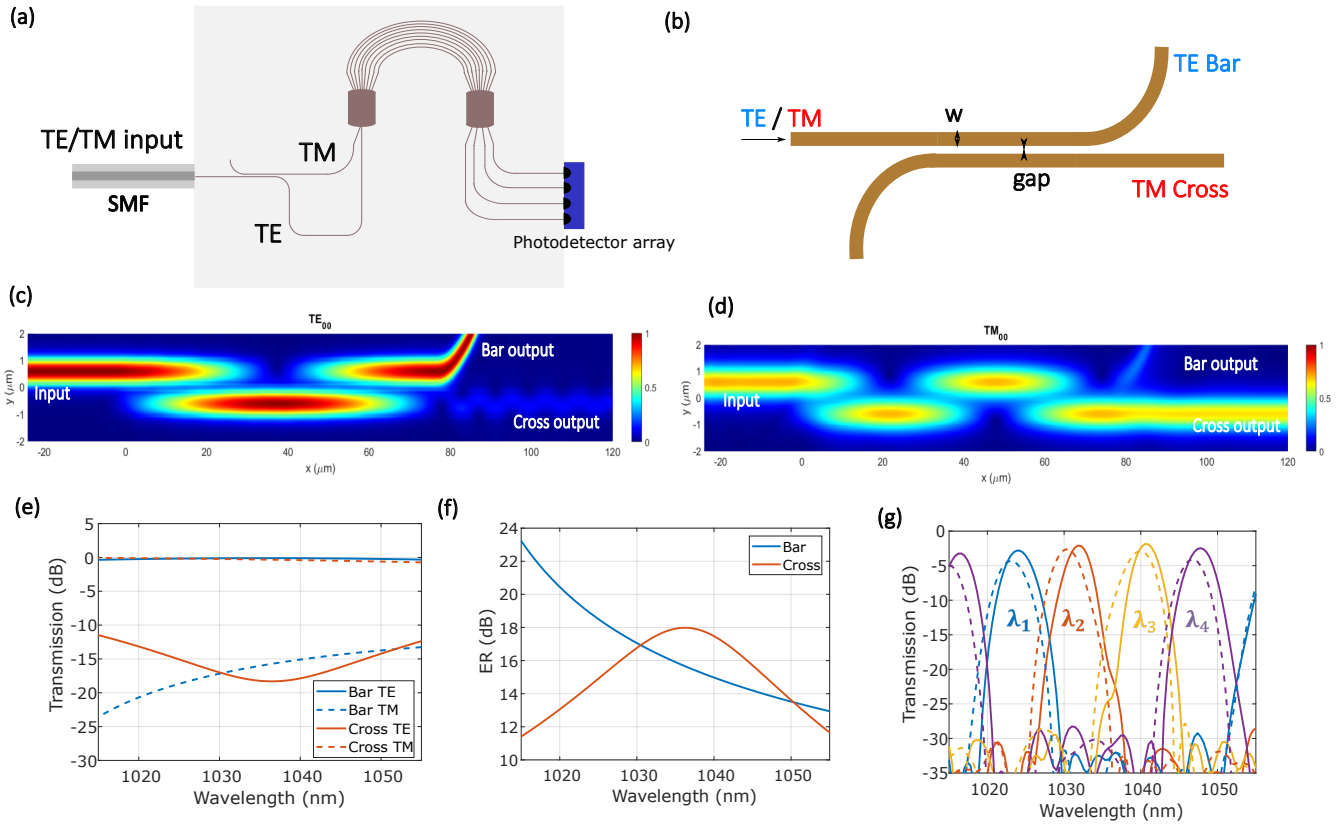

Fig. 1. (a) Scheme of the whole PIC including an AWG and output grating couplers designed for one specific polarization. (b) Scheme of the polarization splitter. The length L of the straight section is 74 μm and the gap between the waveguides is 300 nm. FDTD simulation of the E-field profile of the polarization splitter for (c) TE and (d) TM polarizations. (e) Output transmission of the polarization splitter for TE and TM polarizations. (f) Extinction ratio of the splitter. (g) Simulations of the AWG for TE (continuous lines) and TM (dashed lines) polarizations. Each color corresponds to one specific output channel centered at a specific wavelength: λ_1 = 1023 nm, λ_2 = 1031 nm, λ_3 = 1039 nm and λ_4 = 1047 nm.

change from TE to TM polarization compensates that of the effective index in the FPR region.

Unfortunately, meeting this condition with a waveguide thickness of 160 nm is not possible as the width would be too small to guide the TE_{00} and TM_{00} modes. One possibility to solve the channel mismatch problem due to polarization dispersion consists in cascading a polarization splitter with a rotator at the cross output port, allowing only the TE polarization to thrive. This approach will be investigated in next section.

III. Receiver based on a polarization splitter-rotator and two identical cascaded MZIs

Another solution consists in inserting a rotator at the TM output port of the input polarization splitter [20] to rotate the electric field by 90°, thus converting the TM_{00} input mode into a TE_{00} mode. Hence, the main factor to consider is the polarization conversion efficiency, which is defined as the ratio between the proportion converted into a TE mode and the input TM mode. A compact device that could split and rotate the polarization was demonstrated in [21]. The design principle was based on modifying the width of one of the two waveguides so that the effective index of the TE_{00} of the smallest waveguide matches with that of the effective index of the TM_{00} of the largest waveguide. A similar design was also demonstrated in [22] based on silicon. However, to perform a successful polarization conversion, the material of the top cladding needs to differ from that of the bottom one [21], [22]. Regarding the demultiplexing device, a polarization rotator was inserted in each waveguide in the array section of an AWG in [17] to limit the footprint of the WDM. But this is at the cost of increasing the manufacturing complexity of the PIC. In this section, we propose a solution that decreases the manufacturing complexity of the circuit by using only one rotator at the input.

In this polarization independent receiver design, we consider a polarization splitter-rotator. A demultiplexer based on a cascaded MZI is placed at both outpout ports of the polarization splitter as shown in Figure 2a and b. The cascaded MZI was selected due to its high performance and good tolerance to fabrication deviations [12]. The demultiplexers are identical and designed for the TE polarization. The polarization rotator is placed at the TM output port of the polarization splitter. As only the TE_{00} mode is propagating through the MZIs, the grating coupler could be considered for the output as illustrated in Figure 2a. A receiver design with two 4-wavelength arrays of photodiodes instead of one can be exploited to avoid possible

This article has been accepted for publication in IEEE Photonics Journal. This is the author's version which has not been fully edited and content may change prior to final publication. Citation information: DOI 10.1109/JPHOT.2024.3361802

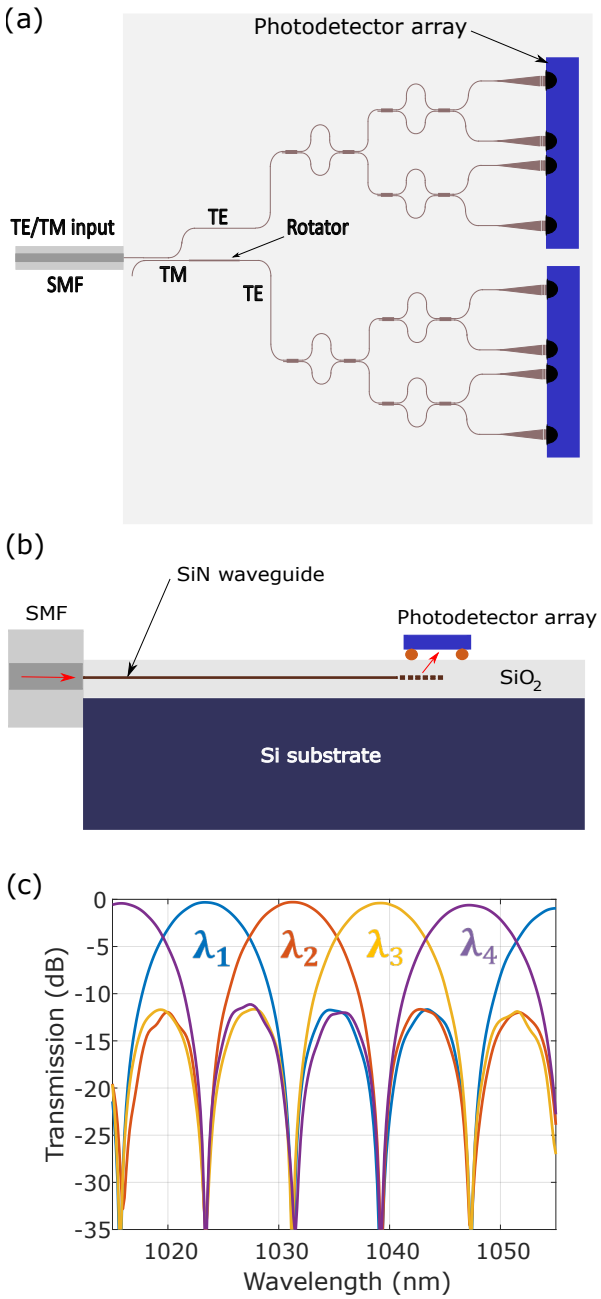

Fig. 2. (a) Scheme of the full receiver based on two identical cascaded MZIs designed for the TE polarization. (b) Side view of the receiver with the SiN waveguides encapsulated in the SiO2 cladding. The red arrows represent the light coming from the fiber and coupled into the array of photodetectors. (c) Transmission of the cascaded MZIs. Each color corresponds to one specific output channel.

interferences from unwanted signals, as well as compensating for polarization dependent losses in the electric domain, after photodetection. The total footprint of the receiver is estimated to be 2200 μm $\times$ 1300 μm, which is slightly larger than the first receiver design proposed in Section II. To obtain a channel spacing of 8 nm, the base length difference between the MZI arms on the first stage is 37.7 μm. The power splitters used are multimode interferometers (MMIs). The simulated

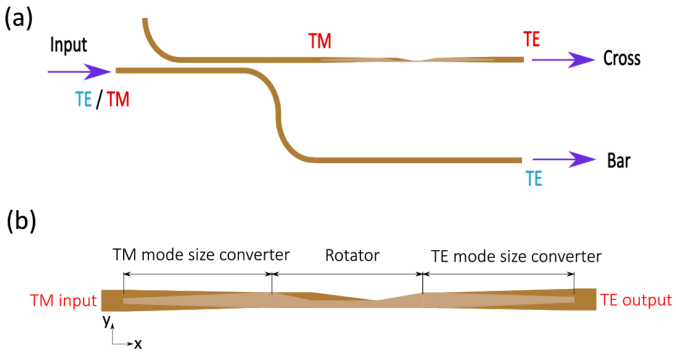

Fig. 3. (a) Scheme of the full polarization splitter/rotator. (b) Zoom on the polrization rotator with the mode size converters.

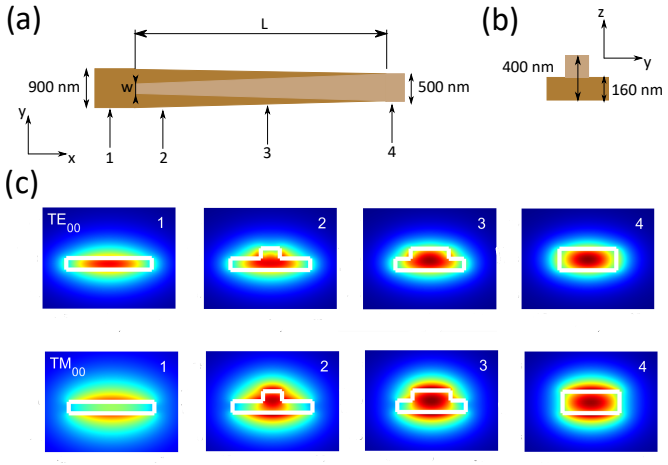

Fig. 4. (a) Top view of the mode size converter. The input and output mode converters have different dimensions denoted as L and w. The length L of the upper linear taper is 25 μm for TE_{00} (output) and 100 μm for TM_{00} (input). The width for both input and output tapers is w = 100 nm. (b) Cross section of the device. The slab is 160 nm thick and the total height is 400 nm. (c) Onsets of the electric field profiles for both polarization.

transmission of the cascaded MZI is plotted in Figure 2c and was carried out with 2.5D-FDTD (varFDTD).

For this receiver platform, we exploit the polarization splitter design from section II and then add a rotator at the TM output port as illustrated in Figure 3. However, such device is more efficient with thick waveguides [17] and would require input and output mode converters [20]. Several techniques exist to rotate the polarization. One of them consists in etching the thick waveguide asymmetrically as in [17], [23]. A device based on silicon was manufactured and performed an extinction ratio of 15 dB with an insertion loss of less than 1 dB in TM-TE conversion [24]. However, the effect of over- and under-etching can degrade the performance of the device [25]. Therefore, another approach consists in a two-layer design [20], [25], enabling fabrication robustness. A slot layer made of SiO_2 is inserted between the two silicon layers in [25]. The effect of misalignment is minimized as slots waveguides serve as an etch stop layer in the final etching process [20]. However, the overall length of this design can exceed 1 mm [20]. Another polarization rotator reported in [5] used a two-core design, the main core made of Si being

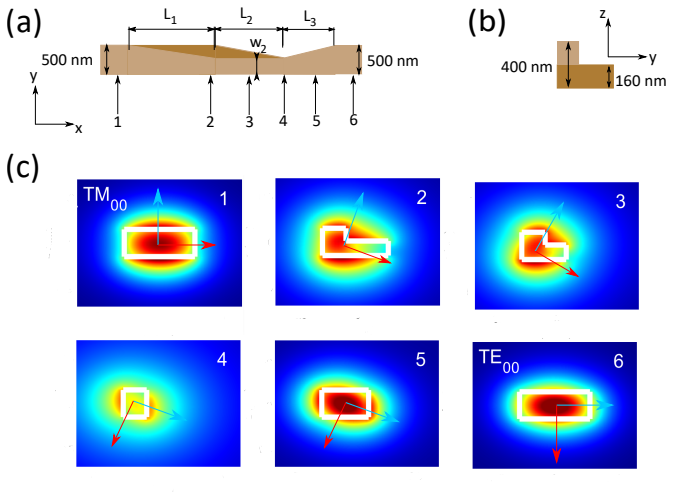

Fig. 5. (a) Top view of the polarization rotator. The optimum values found with EigenMode Expansion (EME) simulations are L_1 = 100 μm, L_2 = 60 μm, L_3 = 20 μm and w_2 = 300 nm. (b) Cross section of the device. The thickness of the slab is the same as for the mode converters and the total height is 400 nm. (c) Onsets of the electric field profile of the guided mode at different sections of the device. The cyan and red arrow respectively represent the direction of the electric and magnetic fields.

inserted in another, larger, made of Si_3N_4.

The architecture used in this work is similar to the designs in [17], [26], [27]. However, designing a rib-rotator based on a 160 nm thick Si_3N_4 is challenging. Therefore, we decided to increase the thickness of the device. For comparison, the rotator in Ref [17] also based on Si_3N_4 material in the O-band uses a 700 nm (wide) × 600 nm (thick) core with a 350 nm thick slab. To reach a TM-TE conversion efficiency above 90 %, the waveguide dimensions need to be properly optimized. The best found waveguide had a width of 500 nm and a thickness of 400 nm. Then, the thickness of the slab also plays a significant role in the conversion efficiency. Here, the selected thickness for the slab is the same as that of the main 900 nm (wide) × 160 nm (thick) waveguide to limit the number of etching steps. Hence, to be adapted for our PIC based on a 900 nm × 160 nm, mode converters must be inserted at the input/output of the rotator. This feature was chosen to limit the propagation loss through the PIC, even though it increases the complexity of the circuit. The other approach, simpler, would be designing the entire PIC based on the 500 nm × 400 nm, but at the cost of higher propagation loss. As the WDM receiver based on the 900 nm × 160 nm waveguide would require only two etching steps and that the accuracy can be controlled with a deviation of a few nm only, we believe that the design is not too limited by the fabrication. Therefore, we opted for this design based on the 900 nm × 160 nm waveguide requiring the use of mode converters. However, with respect to the receiver design in Section II, since Si_3N_4 is deposited with LPCVD, crack barriers and thermal cycling process would be required as cracks can occur for Si_3N_4 films with thicknesses above 350 nm [28]. Indeed, the mode converters and polarization rotator are 400 nm thick after the second etching step.

Figures 4 and 5 illustrate the mode converter and the rotator

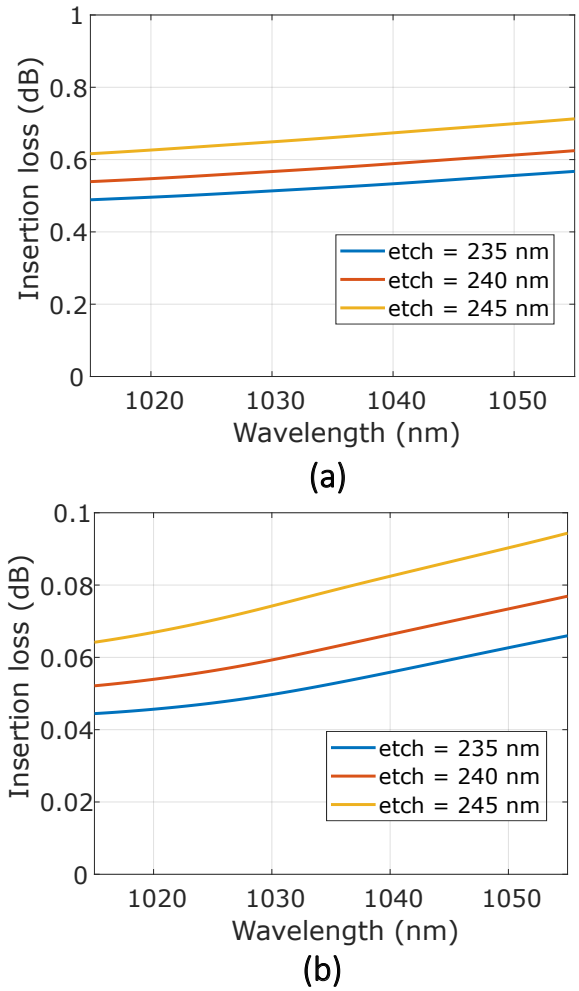

Fig. 6. Insertion losses of the TM (a) and TE (b) mode converters for different etching depths. The TM mode converter is placed at the input port of the rotator and the TE mode converter is placed at the output port.

respectively with the insets of the electric fields of the guided mode through the devices. The length of the tapered section of the mode converter is selected to ensure an adiabatic transition between the waveguides. The length of the input converter, which is adapted for the TM polarization, is 100 μm-long. The output mode converter however, is only 25 μm-long as it is designed for the TE polarization, resulting in a more confined mode in this case. Figure 5c presents the simulated electric field profiles at different section of the rotator for an input TM_{00} mode. A successful rotation can be observed when comparing the first and last electric fields. The main parameters of the device (lengths of the tapering sections, width w_2 of the nanowire) were optimized with EingenMode Expansion (EME) simulations. The optimizations start with a selection of a sufficiently large width w_2 to minimize the insertion loss and primary values for L_1, L_2 and L_3. The lengths are then swept one by one to maximize the conversion efficiency.

Figure 6 presents the impact of etching on the insertion loss of the input (a) and output (b) mode converters, for the TM and

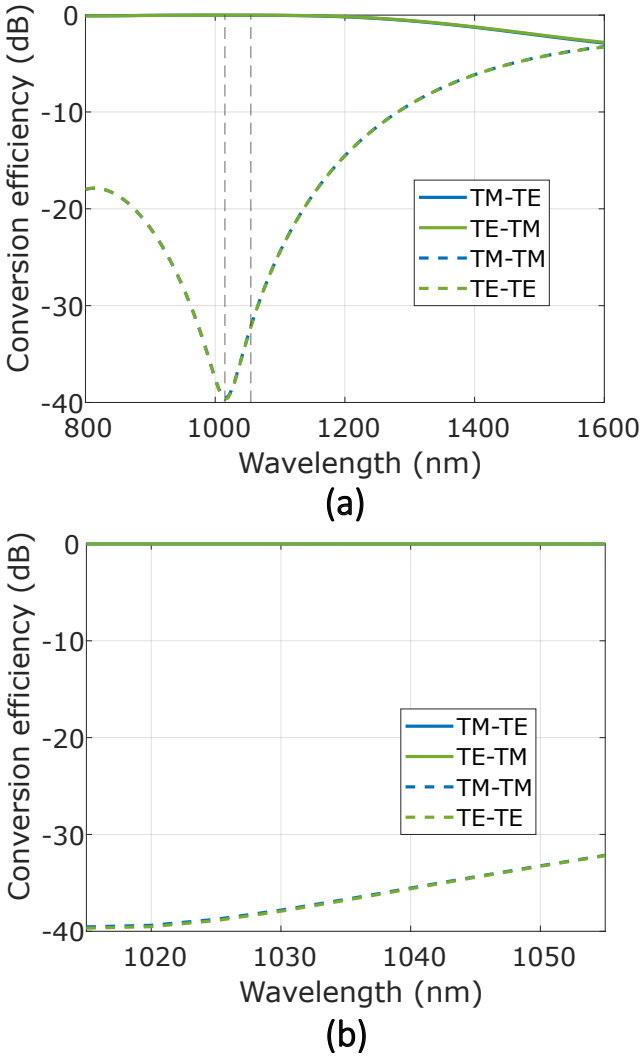

Fig. 7. (a) EME simulations of the polarization rotator. The dashed vertical lines represent the bandwidth of interest. (b) Simulation of the rotator within the bandwidth of interest.

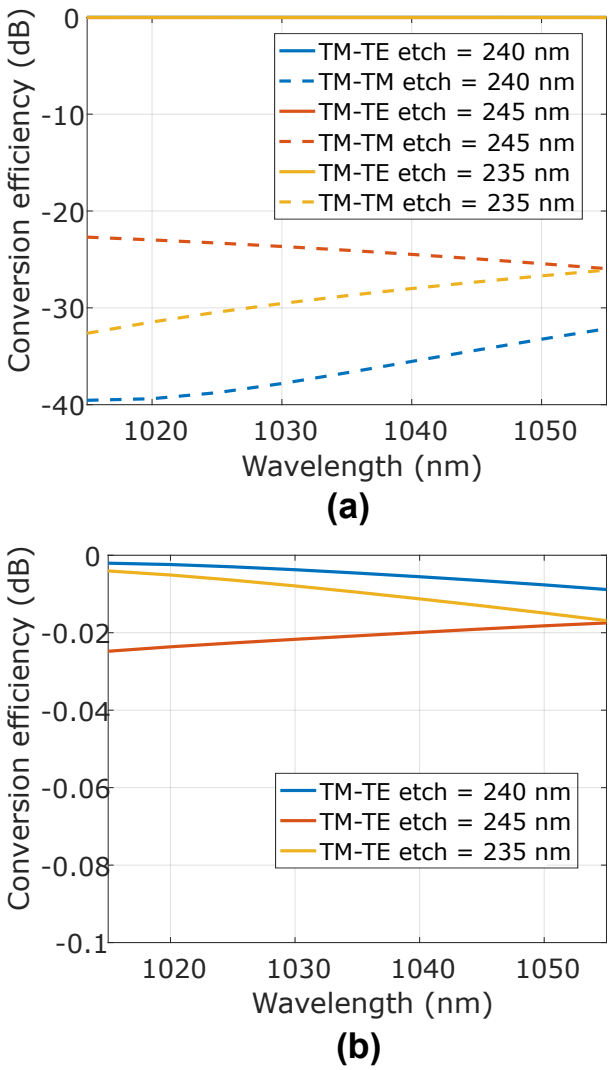

Fig. 8. (a) EME simulations of the impact of the etching depth on the performance of the rotator. (b) Zoom on the simulated TM-TE conversion efficiencies for different etchings.

TE polarization respectively. Overall, the results show that the mode converters are robust to deviations in the etching depth, with the input converter showing insertion losses within 0.8 dB and the output converter within 0.1 dB. The loss is higher for the input converter due to the far weaker confinement of the TM_{00} mode in the 900 nm × 160 nm waveguide, leading to a less effective adiabatic transition into the 500 nm × 400 nm waveguide.

Figure 7 shows the simulated conversion efficiency of the polarization rotator when the device is properly etched at 240 nm. The obtained conversion efficiency at 1035 nm is 99.9 % and an extinction ratio of 40 dB at 1015 nm and 32 dB at 1055 nm. In addition, the TM-TE and TE-TM conversions show a bandwidth large enough to work at wavelengths between 800 and 1200 nm, but the extinction ratio is lower than 20 dB at these wavelengths. The high wavelength dependence of the device is due to the wavelength dependence of the effective index and thus of the modal confinement of the injected mode. To avoid effective index crossing between the TE_{00} and TM_{00} modes [17], we decided to make the nanowire section represented by the parameter w_2 (300 nm) in Figure 5a significantly smaller the device's thickness, which was 400 nm. Shifting the notche's dip towards the center of the bandwidth of interest would require further enlarging w_2 but the extinction ratio's level at 1055 nm (-32 dB) in Figure 7b is good enough for our system, which requires a maximum crosstalk level of -20 dB [12]. A similar TM-TE conversion efficiency higher than 99 % was obtained in Ref [17]. The calculated extinction ratio between the two polarizations is 38 dB. In section II, we saw that the polarization splitter has an extinction ratio of 18 dB in the cross output, (where the rotator is placed) when the input polarization is TE. This signal will then be converted into a TM_{00} mode by the rotator and then transmitted to the demultiplexing device in Figure 2. However, as the demultiplexer is based on a cascaded MZI which is specifically designed for the TE polarization, this signal will be further attenuated.

Figure 8 shows the simulated impact of the etching depth on the device's performance. The rotator shows good robustness to etching variations. In Figure 8a, we observe that the TM-TE conversion remains almost unchanged while the TM-TM conversion increases by 9 dB when under-etched by 5 nm and by 14 dB when over-etched by 5 nm. The zoom on the TM-TE conversion efficiencies in Figure 8b shows that a ±5 nm etching variation has a negligible impact as the efficiency decreases by 0.017 dB in the worst case.

IV. Conclusion

We proposed two integrated receivers based on a thin waveguides. The first design uses an AWG with a polarization splitter based on a straight directional coupler. The receiver has a polarization dependent loss of 1-2 dB depending on the channel and suffers from a slight channel shift of 1 nm in the worst case. This receiver design has an estimated size of 1800 μm × 1300 μm and only requires one array of photodiodes. In addition, only one etching step is required for this receiver. However, it was found in Ref [12] that AWGs are more prone to fabrication defects with respect to MZIs and that the writing time was at least seven fold for a system with 4 channels. Finally, if this receiver only requires one array of photodiode, output edge couplers are more sensitive than grating couplers to possible misalignments between the array and the waveguides of the output channels. Advanced edge coupling designs using multilayers or subwavelength grating structures could be considered to reduce both the coupling and misalignment loss [29].

The second receiver design combines the polarization splitter used from the first design with a partially etched polarization rotator. Since the rotator is based on a 500 nm (width) × 400 nm (thickness) waveguide, which differs from the 900 nm × 160 nm base waveguide, this device requires partially etched mode size converters at the input and at the output ports. The interest of this receiver is the reduction of the fabrication complexity with selecting the thickness of the slab sections of the rotator and of the converters the same as the 900 nm × 160 nm base waveguide. Therefore, only two etching steps are required. The loss from the converters are 0.06 dB for the TE polarization and 0.6 dB for the TM polarization. The devices show in addition good tolerance to deviations in the etching depth. The polarization rotator has a TM-TE conversion efficiency of 99.9 % and an extinction ratio between 30 and 40 dB. The rotator also good robustness to over- and under-etching. To avoid possible interferences coming from unwanted signal, this receiver requires twice the amount of photodiodes with respect to the first design, which increases the cost of manufacturing, but this is compensated by the low complexity of the cascaded MZIs and the relaxed tolerance to misalignment offered by the grating couplers. However, advanced designs with a bottom reflector [3] or using a staircase profile [30] should be considered to reach high coupling efficiencies. Finally, the estimated size of this receiver is 2200 μm × 1300 μm, which is close to the first proposed design.

Acknowledgment

This work was funded by the Swedish Research Council (2016-06077, iTRAN project).

References

[1] M. Girardi, A. Larsson, and V. Torres-Company, "Performance tradeoffs in low-loss Si3N4 waveguides for linear and nonlinear applications," in *European Conference on Integrated Optics*, Milano, Italy, 2022.

[2] J. F. Bauters, M. J. R. Heck, D. John, D. Dai, M.-C. Tien, J. S. Barton, A. Leinse, R. G. Heideman, D. J. Blumenthal, and J. E. Bowers, "Ultra-low-loss high-aspect-ratio (Si3N4) waveguides," *Optics Express*, vol. 19, no. 4, pp. 3163–3174, 2011.

[3] X. Hu, M. Girardi, Z. Ye, P. Muñoz, A. Larsson, and V. Torres-Company, "Si3N4 photonic integration platform at 1 μm for optical interconnect," *Optics Express*, vol. 28, no. 9, pp. 13 019–13 031, 2020.

[4] H. Fukuda, K. Yamada, T. Tsuchizawa, T. Watanabe, H. Shinojima, and S. ichi Itabashi, "Ultrasmall polarization splitter based on silicon wire waveguides," *Optics Express*, vol. 14, no. 25, 2006.

[5] H. Fukuda, K. Yamada, T. Tsuchizawa, T. Watanabe, H. Shinojima, and S. Itabashi, "Silicon photonic circuit with polarization diversity," *Optics Express*, vol. 16, no. 7, pp. 4872–4880, 2008.

[6] K. Yamada, H. Fukuda, T. Tsuchizawa, T. Watanabe, and S. Itabashi, "Polarization-independent ultrasmall silicon photonic circuits," *NTT Technical Review*, vol. 8, no. 2, 2010.

[7] J. C. Mikkelsen, A. Bois, T. Lordello, D. Mahgerefteh, S. Menezo, and J. K. S. Poon, "Polarization-insensitive silicon nitride Mach-Zehnder lattice wavelength demultiplexers for CWDM in the O-band," *Optics Express*, vol. 26, no. 23, pp. 30 076–30 084, 2018.

[8] E. Simpanen, J. Gustavsson, E. Haglund, E. Haglund, A. Larsson, W. Sorin, S. Mathai, and M. Tan, "1060 nm single-mode vertical-cavity surface-emitting laser operating at 50 Gbit/s data rate," *Electronics Letters*, vol. 53, no. 13, pp. 869–871, 2017.

[9] A. Larsson, E. Simpanen, J. Gustavsson, E. Haglund, E. Haglund, T. Lengyel, P. Andrekson, W. Sorin, S. Mathai, M. Tan, and S. Bickham, "1060 nm VCSELs for long-reach optical interconnects," *Elsevier Optical Fiber Technology*, vol. 44, pp. 36–42, 2018.

[10] M. Jahed, J. S. Gustavsson, and A. Larsson, "VCSEL wavelength setting by intra-cavity phase tuning - numerical analysis and experimental verification," *IEEE Journal of Quantum Electronics*, vol. 57, no. 6, pp. 1–7, 2021.

[11] M.-J. Li, "Novel optical fibers for data center applications," in *Proceedings of SPIE*, San Francisco, California, United States, 2016.

[12] A. Caut, M. Girardi, V. Torres-Company, A. Larsson, and M. Karlsson, "Channel scalability of silicon nitride (de-)multiplexers for optical interconnects at 1 μm," *Journal of Lightwave Technology*, 2023.

[13] P. Muñoz, G. Micó, L. A. Bru, D. Pastor, D. Pérez, J. D. Doménech, J. Fernández, R. Baños, B. Gargallo, R. Alemany, A. M. Sánchez, J. M. Cirera, R. Mas, and C. Domínguez, "Silicon nitride photonic integration platforms for visible, near-infrared and mid-infrared applications," *Sensors*, vol. 17, no. 9, 2017.

[14] T. Akiyama, S. Oda, Y. Nakasha, A. Hayakawa, S. Tanaka, Y. Tanaka, and T. Hoshida, "Cascaded amz triplets: a class of demultiplexers having a monitor and control scheme enabling dense wdm on si nano-waveguide pics with ultraslow crosstalk and high spectral efficiency," *Optics Express*, vol. 29, no. 6, pp. 7966–7985, 2021.

[15] S. S. Cheung and M. R. T. Tan, "Silicon nitride (Si3N4) (de-)multiplexers for 1-μm CWDM optical interconnects," *Journal of Lightwave Technology*, vol. 38, no. 13, pp. 3404–3413, 2020.

[16] Q. Han, J. St-Yves, Y. Chen, M. Ménard, and W. Shi, "Polarization-insensitive silicon nitride arrayed waveguide grating," *Optics Letters*, vol. 44, no. 16, pp. 3976–3979, 2019.

[17] S. Guerber, C. A. Alonso-Ramos, X. L. Roux, N. Vulliet, E. Cassan, D. Marris-Morini, F. Boeuf, and L. Vivien, "Polarization independent and temperature tolerant AWG based on a silicon nitride platform," *Optics Letters*, vol. 45, no. 23, pp. 6559–6562, 2020.

[18] Y. Doi, T. Yoshimatsu, and Y. Nakanishi, "Progress in multi-wavelength receiver integration with arrayed waveguide gratings," *NTT Technical Review*, vol. 19, no. 4, 2021.

[19] H. Zhang, Y. Huang, S. Das, C. Li, M. Yu, P. G.-Q. Lo, M. Hong, and J. Thong, "Polarization splitter using horizontal slot waveguide," *Optics Express*, vol. 21, no. 3, 2012.

[20] B. Troia, F. D. Leonardis, M. Lanzafame, T. Muciaccia, G. Grasso, G. Giannoccaro, C. E. Campanella, and V. M. N. Passaro, "Design and optimization of polarization splitting and rotating devices in silicon-on-insulator technology," *Advances in OptoElectronics*, 2014.

[21] Y. Zhang, Y. He, X. Jiang, B. Liu, C. Qiu, Y. Su, and R. A. Soref, "Ultra-compact and highly efficient silicon polarization splitter and rotator," *APL Photonics*, vol. 1, no. 091304, 2016.

[22] D. Dai and J. Bowers, "Novel concept for ultracompact polarization splitter-rotator based on silicon nanowires," *Optics Express*, vol. 19, no. 11, 2011.

[23] C. Alonso-Ramos, S. R. Garcia, A. O. Moñux, I. M. Fernández, R. Zhang, H.-G. Bach, and M. Schell, "Integrated polarization rotator for ultra-high-speed optical communication systems," in *SPIE OPTO*, 2012.

[24] M. Y. J. Zhang, G.-Q. P. Lo, and D.-L. Kwong, "Silicon-waveguide-based mode evolution polarization rotator," *IEEE Journal of Selected Topics in Quantum Electronics*, vol. 16, no. 1, pp. 53–60, 2010.

[25] H. Zhang, S. Das, J. Zhang, Y. Huang, C. Li, S. Chen, H. Zhou, M. Yu, P. G.-Q. Lo, and J. T. L. Thong, "Efficient and broadband polarization rotator using horizontal slot waveguide for silicon photonics," *Applied Physics Letters*, vol. 101, no. 021105, 2012.

[26] K. Ogawa and K. Nishide, "Is silicon photonics a competitive technology to enable better and highly performing networks?" in *Silicon Photonics III*, L. Pavensi and D. J. Lockwood, Eds. Springer, 2016.

[27] K. G. et al., "Low-loss partial rib polarization rotator consisting only of silicon core and silica cladding," *Optics Express*, vol. 40, no. 7, 2015.

[28] Z. Ye, K. Twayana, P. A. Andrekson, and V. Torres-Company, "High-Q si3n4 microresonators based on a subtractive processing for kerr nonlinear optics," *Optics Express*, vol. 27, no. 24, 2019.

[29] X. Mu, S. Wu, L. Cheng, and H. Fu, "Edge couplers in silicon photonic integrated circuits: A review," *MPDI: applied sciences*, vol. 10, no. 1538, 2020.

[30] M. Jahed, A. Caut, J. Goyvaerts, M. Rensing, M. Karlsson, A. Larsson, G. Roelkens, R. Baets, and P. O'Brien, "Angled flip-chip integration of VCSELs on silicon photonic integrated circuits," *Journal of Lightwave Technology*, vol. 40, no. 15, pp. 5190–5200, 2022.